Journal of the Ceramic Society of Japan 114 [11] 918–922 (2006)

Paper

Synthesis and Photoluminescent Properties of Wurtzite ZnS Nanorods by Hydrothermal and Co-precipitation Methods

Pai-Chia KUO, Hong-Wen WANG* and San-Yuan CHEN

Department of Materials Science and Engineering, National Chiao-Tung University, Hsinchu 300, Taiwan, R.O.C.
**Department of Chemistry, Chung-Yuan Christian University, Chungli, 320, Taiwan, R.O.C.*

Nanorods of wurtzite ZnS were synthesized by a hydrothermal method at 200°C and a co-precipitation method at room temperature in the presence of ethylenediamine (en) aqueous solutions. It was found that the wurtzite ZnS nanorods with uniform diameter around 80±20 nm, length about 300±100 nanometer appears at a proper concentration of en, unit [Zn] : [S] ratio, and an appropriate duration by the hydrothermal method. Much longer wurtzite ZnS nanorods with length from 300 to 2000 nm and diameter from 80 to 200 nm were obtained via the co-precipitation method. A very minor undecomposed ZnS·0.5en phase coexisted with the wurtzite ZnS nanorods in the co-precipitation method was identified and arguably thought to be due to the low temperature used. ZnO coated ZnS core-shell structures were successfully fabricated by annealing the ZnS nanorods in an oxygen flow at 650°C for 3–5 min. The coating of ZnO layer on ZnS nanorods results in a significant increase of photoluminescence (PL) intensity (30 times) at 490–500 nm visible regions for those of hydrothermal method and mild increase (double) for those of co-precipitation method.

[Received July 9, 2006; Accepted October 19, 2006]

Key-words : *Hydrothermal, Co-precipitation, ZnS/ZnO, Core-shell, Nanorods*

1. Introduction

ZnS has been of great research interest as a result of its unique applications in optoelectronic and luminescent devices.[1)–3)] For these applications, the crystallographic structures and morphology control of ZnS are critical to tune their luminescent properties. For instance, the wurtzite ZnS nanorods exhibit much narrower and stronger blue emission as compared to the cubic ZnS nanograins. However, hexagonal wurtzite ZnS is a thermodynamically metastable phase, and cubic sphalerite ZnS is the most stable phase under ambient conditions. It was reported that the hexagonal structure could be transformed spontaneously to the cubic by contact with some organic molecules at ambient temperature.[4)] Conversely, bulk cubic ZnS can transform to the hexagonal structure over 1020°C.[5),6)] Even for nanocrystalline cubic sphalerite ZnS (2.8 nm), the transformation to wurtzite could be achieved in a vacuum at a temperature over 400°C.[7)] Generally, the hydrothermal route leads to the formation of cubic ZnS in nature. The attempt to prepare wurtzite ZnS nanorods using enthylenediamine (en) as liquid media, produces a complex compound ZnS.0.5en,[8),9)] which need to be further decomposed to wurtzite ZnS in an inert atmosphere at temperatures above 350°C.[8)–10)] Therefore, it is a great challenge to synthesize wurtzite ZnS nanorods and retard its transformation to the cubic phase under milder conditions, such as under hydrothermal or room temperature conditions.

The surface control of ZnS nanoparticles is another important factor for their luminescent properties, because the luminescence efficiency of ZnS nanoparticles is inferior due to the increased surface area and proportionately higher unsaturated dangling bond rated non-radiative recombination sites or some other kinds of dead layers due to surface defects. Successes in preparing ZnO or ITO capped ZnS (denoted as core/shell) nanostructure materials and their enhanced luminescent properties were reported,[8),9),11)–18)] which is based on their saturated dangling bonds and substantially decrease non-radiative centers (dead layers), moreover, they can also withstand high temperature treatments and electron bombardment without increasing the ZnS particle size or time dependent luminescence degradation (or aging effects).

Herein, we report simple approaches to synthesize wurtzite ZnS nanorods using hydrothermal and co-precipitation process in aqueous solution at low temperature. In order to tune the surface of ZnS nanorods, ZnO/ZnS core-shell structures were successfully fabricated by annealing the ZnS nanorods in an oxygen flow. Further, the photoluminescent properties of ZnS nanorods and their ZnO/ZnS core-shell dependent-luminescent properties are investigated.

2. Experimental procedure

The starting precursors were zinc acetate dihydrate ($Zn(CH_3COO)_2(2H_2O)$), and thiourea (CH_4N_2S) for the hydrothermal process[8)] and zinc acetate dihydrate and sodium sulfide nona-hydrate for the co-precipitation process (co-ppt) which was a modification from literature,[19)] respectively. All the chemicals were analytical grade and used as received. Equal moles (0.8M) of zinc acetate and thiourea were mixed with ethylenediamine (en, $H_2NCH_2CH_2NH_2$) solution in an autoclave and sealed within a stainless container. The concentrations of ethylenediamine were varied from 12%, 40%, 67% and 90% (to the total volume of solution, 100 ml), respectively. I.e. the concentration of en in the reaction medium is described as a volume ratio in x en to $(100-x)$ H_2O. The hydrothermal process was carried out at 200°C for 2–12 h. The final products were filtered and dried in an oven at 65°C for 2 h. For the co-precipitation process, 0.8 M zinc acetate and sodium sulfide nona-hydrate were prepared into solutions individually. The co-precipitation process was performed by dropping and stirring these two solutions in 1 : 1 ratio into a 67% ethylenediamine solution in a speed of approximately 2 ml/min. The precipitates were put away for 12 h in a hood and finally collected by filtering and dried in an oven at 65°C for 2 h. For the formation of ZnS–ZnO core-shell structures, ZnO layer was grown on the ZnS nanorods by annealing in oxygen at 200–700°C for 1–5 min in a tube furnace.

Crystalline information was obtained using X-ray diffractometry (XRD, M18XHF MAC Science, Japan) equipped with a copper target ($\lambda_{K\alpha 1}=1.5405$ Å). The scanning rate was 6°/min from $2\theta=10°$ to 60° and the operation voltage and current of XRD were 50 kV and 100 mA, respectively. A scanning

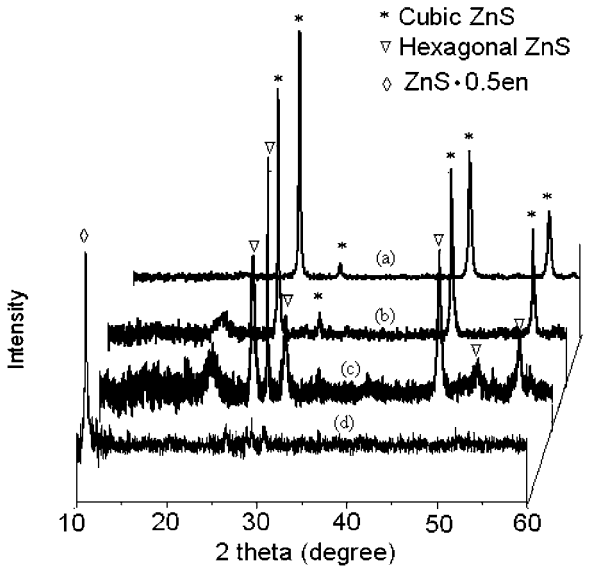

Fig. 1. Effect of concentration of ethylenediamine (en) on the final crystallization of ZnS powders via the hydrothermal process. (a) 12%, (b) 40%, (c) 67% and (d) 90% of en. It is clear that well crystallized hexagonal ZnS could be obtained using 67% en.

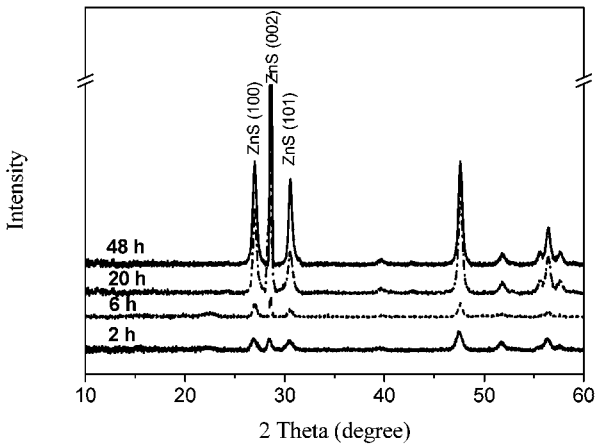

Fig. 2. Formation of ZnS nanorods vis hydrothermal process, from bottom to top, 2 h, 6 h, 20 h, and 48 h.

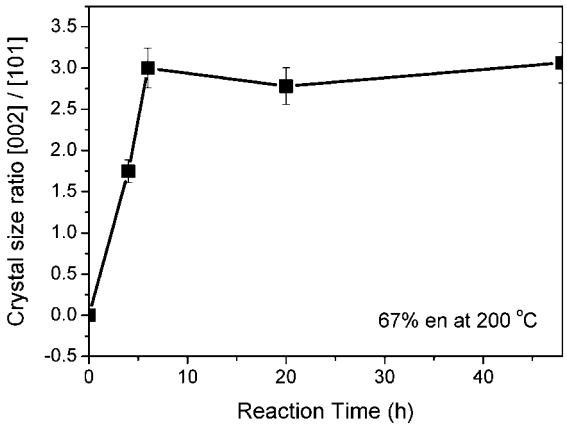

Fig. 3. Crystal growth ratio of [200]/[101] during hydrothermal process.

electron microscope (SEM, Hitachi S–4000) at 30 kV and transmission electron microscope (TEM, model TECANAI 20, Phillips) at 120 kV was employed to reveal the morphologies as well as the diffraction patterns (via selected area electron diffraction, SAED of TEM) of nanorods. A photoluminescence spectrometer was used to evaluate the properties of luminescence of final products. Photoluminescence (PL) measurement was performed by the excitation from 325 nm He–Cd laser at room temperature.

3. Results and discussion

3.1 ZnS nanorods via hydrothermal process

The effect of ethylenediamine (en) on the formation of wurtzite ZnS was shown in **Fig. 1**. When the concentrations of en were 12% and 40%, ZnS was cubic phase (Figs. 1(a) and (b)). However, when 67% of en was used, hexagonal phase of wurtzite ZnS formed (Fig. 1(c)). As the concentration of en increased to 90%, the products were ZnS·0.5en. (Fig. 1 (d)). It was suggested[8] that SCMT (solvent coordination molecular template) mechanism may not happen when low concentration en was used (12% and 40%) and the products were cubic ZnS. When high concentration of en (90%) was used, however, the reaction ZnS·0.5en = ZnS + 1/2 en, could not simply go forward. Because of the chemical equilibrium between ZnS·0.5en and ZnS, ZnS·0.5en is not easily decomposed to ZnS completely in a medium with a high en concentration, especially in pure en solvent. We also changed the starting precursors $[Zn^{+2}]/[S^{-2}]$ ratio to 1/4 and 4/1 in 67% en solution, however, in these cases, cubic ZnS nanoparticles resulted. From above experiments, we confirmed that the wurtzite ZnS nanorods would only form in a proper $[Zn^{+2}]/[S^{-2}]$ ratio (1 : 1) and en concentration (67%).

The duration of hydrothermal process also has a profound effect on the crystal growth of ZnS nanorods. **Figure 2** shows the XRD results for the duration 2 h, 6 h, 20 h, and 48 h at 200°C using 67% en as solvent. It is clear that (110)·(002)·(101) peaks of hexagonal crystals were enhanced at longer durations. In order to understand the growth rate in different directions of crystal, Scherrer's equation was used to transform X-ray intensities of [002] and [101] into growth rate of crystal in these two directions as a function of time. i.e.

$$t = \frac{0.9\lambda}{B\cos\theta_B}$$

where t : length of crystal in a specific direction;
λ : wave length of X-ray (1.5402 Å for Cu target);
B: width of half height of X-ray diffraction peaks;
θ_B: two theta angle of diffraction peaks.

Figure 3 shows the ratio of growth rate in direction [002] over [101]. It is clear that during the hydrothermal process, growth rate in [002] direction is faster than that of [101]. i.e. In our preparation condition, 67% en solution, ZnS crystals prefer to grow in [002] direction and form 1-D nanorods. The aspect ratio [002]/[101] saturates at 3 after 6 h. Longer duration seems have little effect on the aspect ratio, but crystallinity of ZnS nanorods becomes strong as XRD shown in Fig. 2. The morphology of wurtzite ZnS nanorods is shown in **Figs. 4**(a) and (b). The ZnS nanorods are about 200–400 nanometers in length and around 80 ± 20 nm in diameter. These morphologies are repeatedly confirmed and exhibited consistence in the observation of SEM as well as TEM. The selected area electron diffraction (SAED) in up-right corner of Fig. 2(b) demonstrates the formation of single crystal of wurtzite ZnS

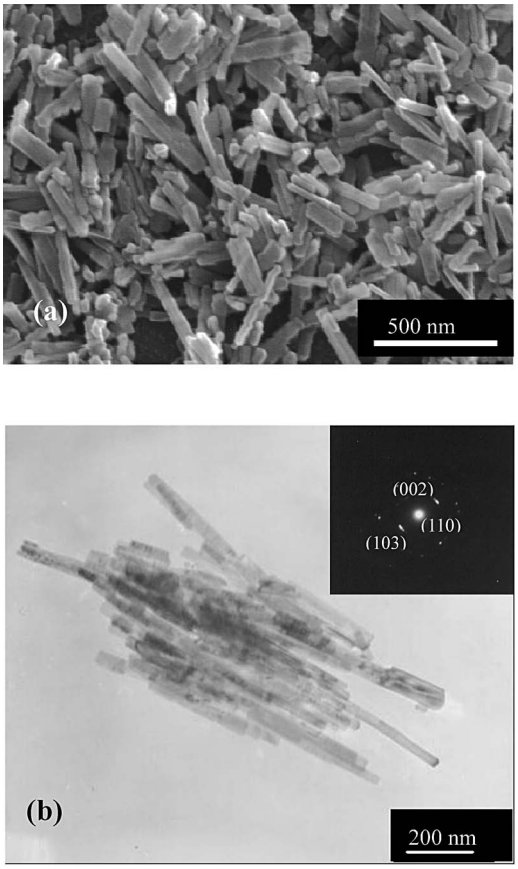

Fig. 4. (a) SEM micrograph, (b) TEM micrograph and upper right corner, SAED for ZnS nanorods obtained by hydrothermal process.

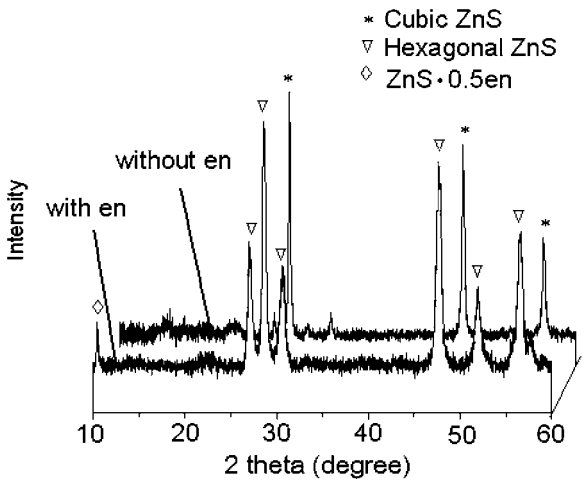

Fig. 5. ZnS phase formation via co-precipitation method.

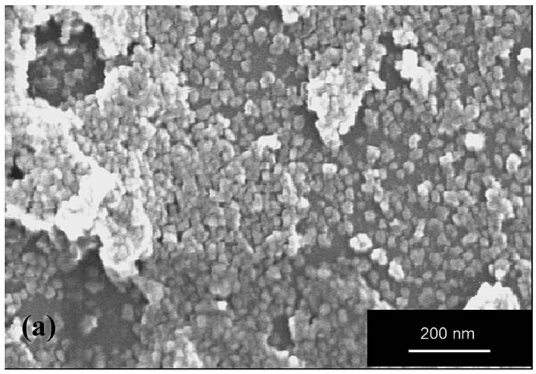

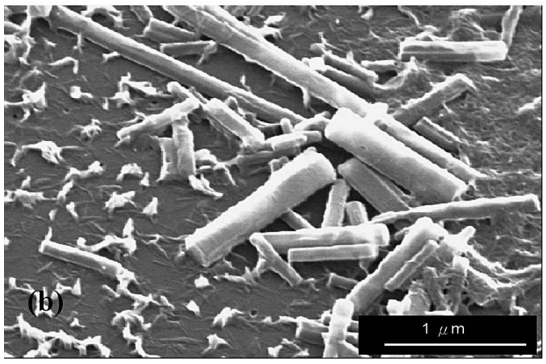

Fig. 6. ZnS nano-materials obtained via co-precipitation (a) without using 67% en, and (b) with the use of 67% en.

nanorods.

3.2 ZnS nanorods via co-precipitation

Co-ppt method was employed intentionally and anticipated to form wurtzite ZnS nanorods at room temperature. Equal moles of Na_2S and zinc acetate (0.8 M) were mixed and precipitates formed according following possible reactions:[19]

$$Na_2S \cdot 2H_2O + Zn(CH_3COO)_2 \cdot 9H_2O \longrightarrow ZnS + 2NaCH_3COO + 11H_2O$$

Cubic ZnS nanoparticles with 10–50 nm in diameter were obtained without using en, as the XRD results shown in **Fig. 5**. However, by using 67% en as the precipitating solution, hexagonal wurtzite ZnS nanorods were readily formed with a minor ZnS·0.5en phase. It is understandable that ZnS·0.5en phase only decomposed at certain high temperature (>180°C) and proper concentration[8),10)] and is difficult to completely transform into ZnS at room temperature. **Figures 6**(a) and (b) show the different morphologies of cubic ZnS nanoparticles and wurtzite ZnS nanorods via co-ppt method, respectively. Diameter of wurtzite ZnS nanorods varying from 80 nm to 200 nm and length from 300 nm to 2 μm were estimated from these micrographs. However, from the area of the XRD peaks in Fig. 5, ZnS·0.5en is very minor and the majority is wurtzite ZnS nanorods. Therefore, we believed that formation of wurtzite ZnS nanorod via co-ppt at room temperature is feasible, only the processing conditions need to be optimized. From the results shown above, it is clear that hydrothermal process produces single wurtzite ZnS nanorods with uniform crystal sizes, while co-ppt results in wurtzite ZnS nanorods with minor cubic phase and somewhat varied and larger rod sizes. The major reason for this difference is thought to be due to the pressure and high temperature used in hydrothermal process, which greatly facilitates uniform nucleation and growth.

3.3 Enhanced photoluminescence on ZnS/ZnO core-shell nanorods

Annealing ZnS nanorods at 650°C under oxygen will form a thin ZnO shell layer on the surface of ZnS, making these nanorods core-shell structures. **Figure 7**(a) shows the crystallization of ZnO phase on hydrothermal ZnS nanorods at different annealing temperatures from 200–700°C for 5 min. When the annealing temperatures are lower than 650°C, ZnS is

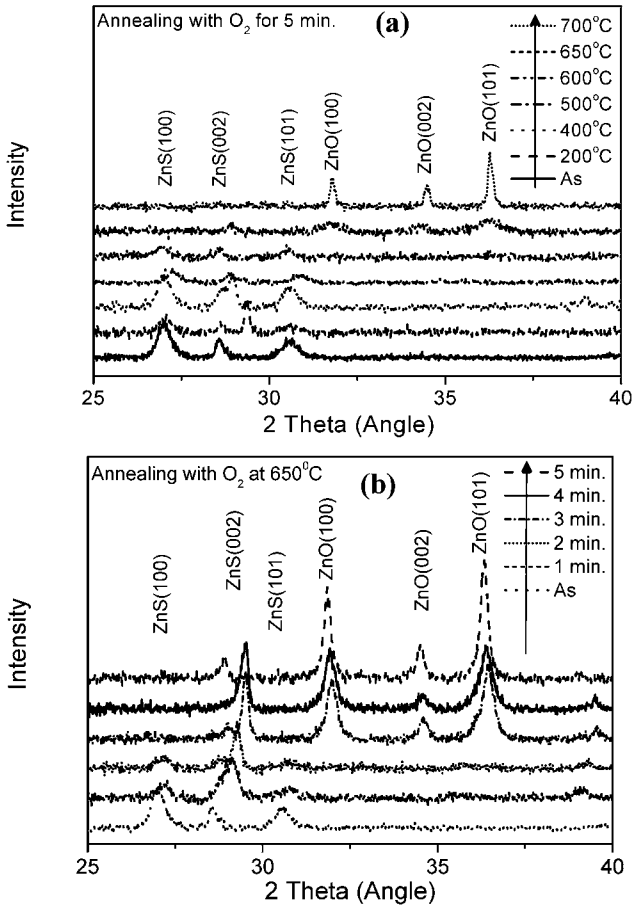

Fig. 7. XRD for the ZnS nanorods annealed in oxygen at (a) different temperatures for 5 min, (b) at 650°C for different durations.

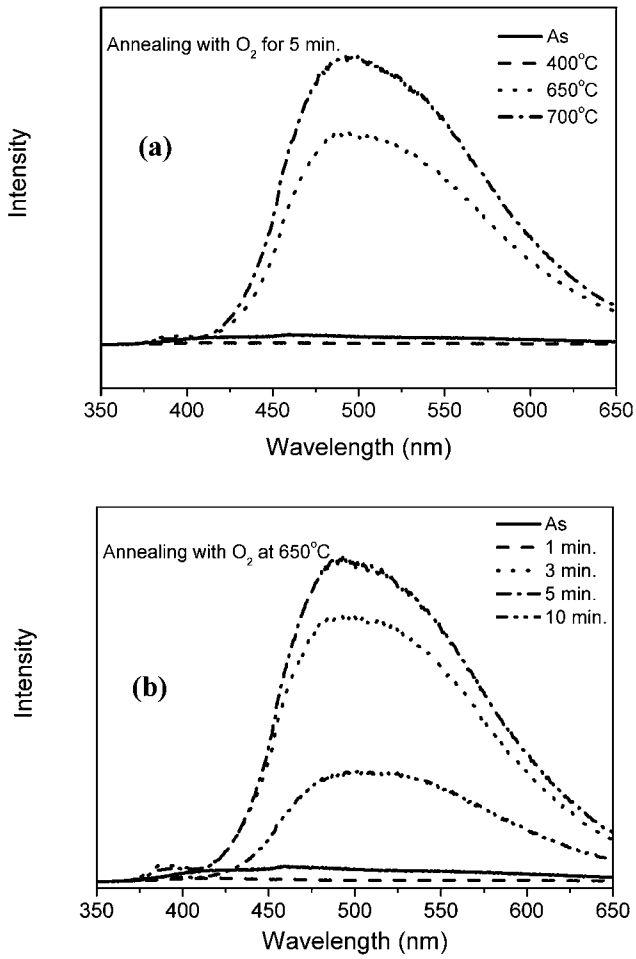

Fig. 8. PL of ZnS nanorods annealed in oxygen, (a) at different temperatures for 5 min, (b) at 650°C for different durations.

the major phase. However, ZnS phase almost disappears and ZnO phase appears when temperature goes higher than 650°C. The crystalline phases of samples after annealing at 650°C for 1–5 min are shown in Fig. 7(b). The formation of ZnO phase during annealing in oxygen is not evident until the duration is longer than 3 min, where ZnS peaks decrease. The ZnS peaks did not completely disappear even the annealing was performed for 5 min at 650°C. However, the ZnO phase was clear at 3–5 min at 650°C. It is believed that the ZnS–ZnO core-shell nanorods was formed for annealing time over 3 min. The PL response for the ZnS nanorods synthesized from en hydrothermal process with/without oxygenation was shown in **Fig. 8** (a). Figure 8(a) shows enhanced peaks of PL around 500 nm for sample annealed at 650°C and 700°C. This is total contribution from both ZnS and ZnO. The width of half height of PL is about 150 nm, which is quite broad, and is believed due to defects which is not associated with central radiation at 500 nm such as zinc vacancies, sulfur vacancies and dangling sulfur bonds at the interface of ZnS crystals.[19] For the annealing at 400°C, the intensity of PL is less than that of non-annealed ZnS. This could be attributed to the oxygenation of the surface of ZnS, and PL of ZnS decreased as the oxygen atom occupied the position of sulfur. When the annealing temperature increases, these defects were mostly eliminated due to well crystallization. The visible radiation at 500 nm was enhanced more than 30 times compared to their original ZnS nanorods. The PL intensity for specimens obtained from en hydrothermal process and annealed at 650°C for 1, 3, 5, and 10 min was also shown in Fig. 8(b). PL was enhanced after annealing at 650°C for 3–5 min. However, after 10 min, PL was greatly reduced due to the conversion of most ZnS to ZnO. In the case of co-ppt process, the core-shell structure also enhanced PL of ZnS nanorods at 500 nm, however, only about twice stronger (not shown). We attribute this mild enhancement of PL from products via co-ppt process to their much larger and scattered crystal sizes as shown in Fig. 6(b).

It was well known that the emission and efficiency are very sensitive to the nature of the nanoparticle surface, due to the presence of gap surface states arising from surface non-stoichiometry, unsaturated bonds, etc. Evidently, the capping effect of ZnO shell reduced the number of dangling bonds on the nanorod's surface which was believed to provide surface trap states for nonradiative recombination and enhance the luminescent efficiency. But from the broad PL band in Fig. 8, it seems that the contribution of the surface-related nonradiative recombination is still obvious. The possible reason might be that the dead layer which was passivated by ZnO shell was not completely eliminated. However, the PL intensity was greatly enhanced after ZnO capping. A possible reason is the capping stress proposed by Karar.[14] The study of Karar on ZnS/ZnO core-shell nanoparticles shows that the maximum PL is observed for 30% ZnO capping (proper thickness of ZnO) but lower PL for thinner or thicker shell thickness. Due to the capping related stress, the corresponding luminescent energy levels may be slightly altered due to a small variation in

lattice parameters, leading to more efficient luminescent transitions, giving higher and sharper PL peaks.[20)-22)] In the present case, in addition to effective passivation, the capping stress might be also important for the enhancement of PL. The effectiveness of passivation and capping stress is more profoundly in the hydrothermal case than in the co-ppt case, where uniform size of ZnS and proper capping ZnO shell is more likely achieved in hydrothermal process, in addition to no intermediate phase of ZnS·0.5en. The optimum conditions for the products via co-ppt method at room temperature and its PL performance deserve more investigations.

4. Conclusion

Wurtzite ZnS nanorods have been synthesized via a hydrothermal process as well as a simple co-precipitation (co-ppt) method. However, for the co-ppt method carried out at room temperature, very minor intermediate compound ZnS·0.5 en remains due to incomplete decomposition. The ZnS–ZnO core-shell nanorods are readily obtained by annealing ZnS nanorods under oxygen at 650°C for 3–5 min. The photoluminescence at the 490–500 nm visible range is greatly enhanced more than 30 times after the formation of ZnO shell on the hydrothermal ZnS nanorods. The effectiveness of passivation and proper capping thickness for the hydrothermal nanorods are thought to be more profoundly than those of co-ppt in the present study. This is attributed to that the hydrothermal method results in uniform size, and single wurtzite phase of ZnS as well as proper capping shell thickness of ZnO after annealing.

Acknowledgements The financial support of this research by the NSC 93–2113–M–033–006 and NSC 93–2216–E–009–005 is gratefully acknowledged.

References

1) Calandra, P., Gofferdi, M. and Liveri, V. T., *Colloids Surf. A*, Vol. 160, pp. 9–13 (1999).
2) Prevenslik, T. V., *J. Lumin.*, Vol. 87, pp. 1210–1212 (2000).
3) Trindade, T., O'Brien, P. and Pickett, N. L., *Chem. Mater.*, Vol. 13, pp. 3843–3858 (2001).
4) Murakoshi, K., Hosokawa, H., Tanaka, N., Saito, M., Wada, Y., Sakata, T., Morib, H. and Yanagida, S., *Chem. Commun.*, pp. 321–322 (1998).
5) Shionoya, S. and Yen, W. M., "Phosphor Handbook," CRC Press, Boca Raton, FL (1999).
6) Brus, L., *IEEE J. Quantum Electron.*, Vol. 22, pp. 1909–1914 (1986)
7) Qadri, S. B., Skelton, E. F., Hsu, D., Dinsmore, A. D., Yang, J., Gray, H. F. and Ratan, B. R., *Phys. Rev. B*, Vol. 60, pp. 9191–9193 (1999).
8) Chen, X., Xu, H., Xu, N., Zhao, F., Lin, W., Lin, G., Fu, Y., Huang, Z., Wang, H. and Wu, M., *Inorg. Chem.*, Vol. 42, pp. 3100–3106 (2003).
9) Deng, Z. X., Wang, C., Sun, X. M. and Li, Y. D., *Inorg. Chem.*, Vol. 41, pp. 869–873 (2002).
10) Yu, S. H. and Yoshimura, M., *Adv. Mater.*, Vol. 14, pp. 296–300 (2002).
11) Dinsmore, A. D., Hsu, D. S., Gray, H. F., Qadri, S. B., Tian, Y. and Ratna, B. B., *Appl. Phys. Lett.*, Vol. 75, pp. 802–804 (1999).
12) Xu, S. J., Chua, S. J., Liu, B., Gan, L. M., Chew, C. H. and Xu, G. Q., *Appl. Phys. Lett.*, Vol. 73, pp. 478–480 (1998).
13) Bhargava, R. N., Gallagher, D., Hong, X. and Nurmikko, A., *Phys. Rev. Lett.*, Vol. 72, pp. 416–419 (1994).
14) Karar, N., Singh, F. and Mehta, B. R., *J. Appl. Phys.*, Vol. 95, pp. 656–660 (2004).
15) Karar, N., Chander, H. and Shivaprasad, S. M., *Appl. Phys. Lett.*, Vol. 85, pp. 5058–5060 (2004).
16) Igarashi, T., Kusunoki, T., Ohno, K., Isobe, T. and Senna, M., *Mater. Res. Bull.*, Vol. 36, pp. 1317–1324 (2001).
17) Ollinger, M., Craciun, V. and Singh, R. K., *Appl. Phys. Lett.*, Vol. 80, pp. 1927–1929 (2002).
18) Alivisatos, A. P., *J. Phys. Chem.*, Vol. 100, pp. 13226–13239 (1996).
19) Wageh, S., Ling, Z. S. and Xu-Rong, X., *J. Cryst. Grow.*, Vol. 255, pp. 332–337 (2003).
20) Bol, A. A., Ferwerda, J., Bergwerff, J. and Meijerink, A., *J. Lumin.*, Vol. 99, pp. 325–334 (2002).
21) Wang, Y. and Herron, N., *J. Phys. Chem.*, Vol. 95, pp. 525–532 (1991).
22) Rodrigues, W., Sakata, O., Lee, T. L., Walko, D. A., Marasco, D. L. and Bedzyk, M. J., *J. Appl. Phys.*, Vol. 88, pp. 2391–2394 (2000).